**Supplemental Document**

PHOTONICS Research

# Axial gradient excitation accelerates volumetric imaging of two-photon microscopy

**YUFENG GAO[1,2,†], XIANYUAN XIA[1,2,†], LINA LIU[1,2], TING WU[1,2], TINGAI CHEN[1,2], JIA YU[1,2], ZHILI XU[3], LIANG WANG[1,2], FEI YAN[3], ZHUO DU[4,5], JUN CHU[1,2], YANG ZHAN[6], BO PENG[7], HUI LI[1,2,8], WEI ZHENG[1,2,9]**

[1]*Research Center for Biomedical Optics and Molecular Imaging, Shenzhen Key Laboratory for Molecular Imaging, Guangdong Provincial Key Laboratory of Biomedical Optical Imaging Technology, Shenzhen Institute of Advanced Technology, Chinese Academy of Sciences, Shenzhen 518055, China*

[2]*CAS Key Laboratory of Health Informatics, Shenzhen Institute of Advanced Technology, Chinese Academy of Sciences, Shenzhen 518055, China*

[3]*Paul C. Lauterbur Research Center for Biomedical Imaging, Institute of Biomedical and Health Engineering, Shenzhen Institute of Advanced Technology, Chinese Academy of Sciences, Shenzhen, 518055, China*

[4]*State Key Laboratory of Molecular Developmental Biology, Institute of Genetics and Developmental Biology, Chinese Academy of Sciences, Beijing 100101, China*

[5]*Key Laboratory of Genetic Network Biology, Institute of Genetics and Developmental Biology, Chinese Academy of Sciences, Beijing 100101, China*

[6]*Brain Cognition and Brain Disease Institute, Shenzhen Institute of Advanced Technology, Chinese Academy of Sciences, Shenzhen 518055, China*

[7]*Centre for Micro Nano Systems and Bionic Medicine, Shenzhen Institute of Advanced Technology, Chinese Academy of Sciences, Shenzhen 518055, China*

[8]*hui.li@siat.ac.cn*

[9]*zhengwei@siat.ac.cn*

*† These authors contributed equally to this work*

# Contents

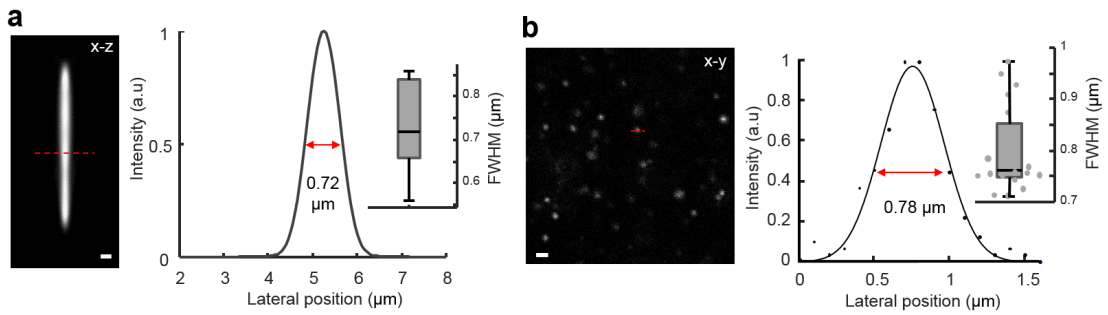


**Fig. S1** Theoretical and experimentally measured lateral resolutions. (**a**) Left, square of simulated point spread function of Grad-TPM ($PSF^2$). Scale bar, 1 μm. Right, lateral profile across middle of $PSF^2$ (dashed red line on left panel), and statistical result of lateral resolutions calculated from different depths of $PSF^2$. Squaring is necessary because intensity of two-photon excitation fluorescence is proportional to square of excitation intensity. (**b**) Left, exemplary image of 100-nm-diameter yellow–green fluorescence beads in gel used for measuring actual resolution of Grad-TPM system. Scale bar, 2 μm. Right, profile across middle of representative bead (dashed red line on left panel) with corresponding Gaussian fitting result and statistical result of lateral resolutions calculated from different beads (n = 20).

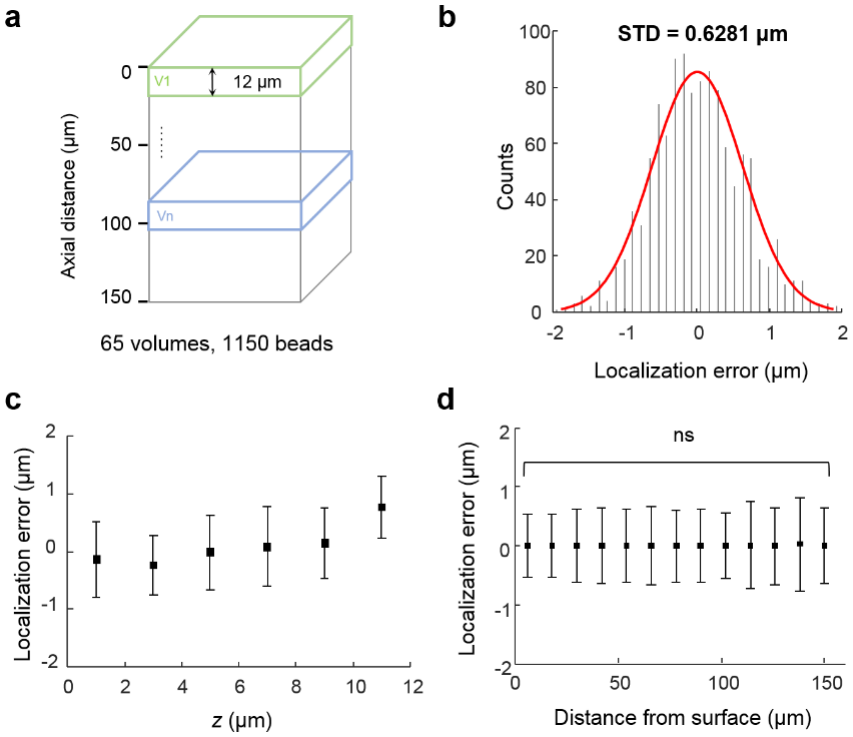


**Fig. S2** Axial localization error analysis on experimental data of Fig. 1c. (**a**) Imaging volume of the experimental data. (**b**) Histogram of the localization error. (**c**) Localization error as a function of depth in a single Grad-TPM volume. (**d**) Localization error as a function of the distance from sample surface.

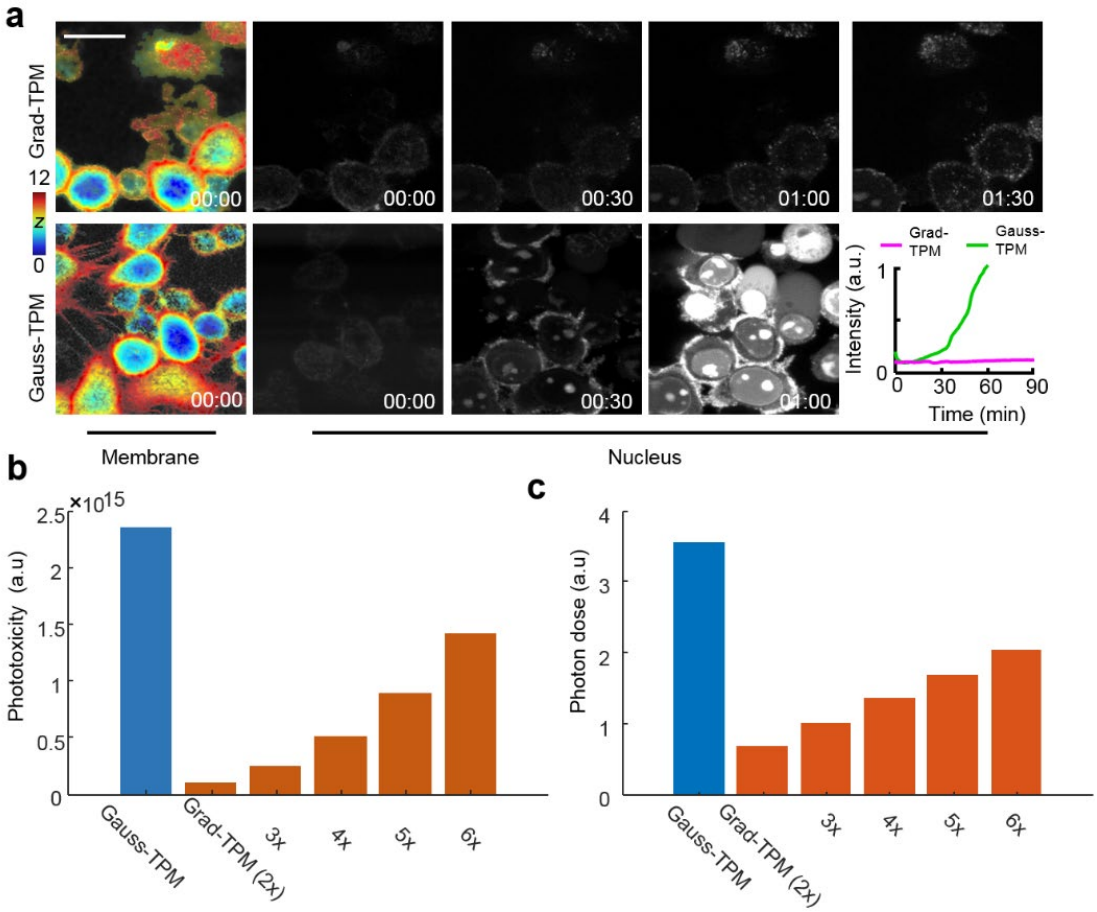


**Fig. S3** Phototoxicity assessment. (**a**) Time-lapse imaging on living HepG2 cells via Grad-TPM shows observably lower phototoxicity compared with traditional Gauss-TPM. Cell membrane and nucleus were labeled with DyLight 488 and PI, respectively. PI cannot cross the membrane of live cells and appear bright only if it binds to the nucleic acids after the cell is dead. Lower right graph is created by calculating average intensity of entire nucleus image at each time point. Scale bars, 20 μm. Time is shown at corner as h:min. Units of $z$: μm. (**b**) Theoretical phototoxicity comparison of Grad-TPM and Gauss-TPM. 2-6× indicate that excitation power of Grad-TPM is two to six times that of the Gauss-TPM. **c,** Theoretical photon-dose comparison. In TPM, phototoxicity and photon dose has been shown to scale as $\int I(\vec{x},t)^{2.5}\,dV\,dt$ and $\int I(\vec{x},t)\,dV\,dt$, respectively, where $I(\vec{x},t)$ is the intensity distribution; $V$ the excited volume, and $t$ the time. Here, we used a cylindrical volume of a radius of 6 μm and a height of 30 μm, and took the focal point as the coordinate center.

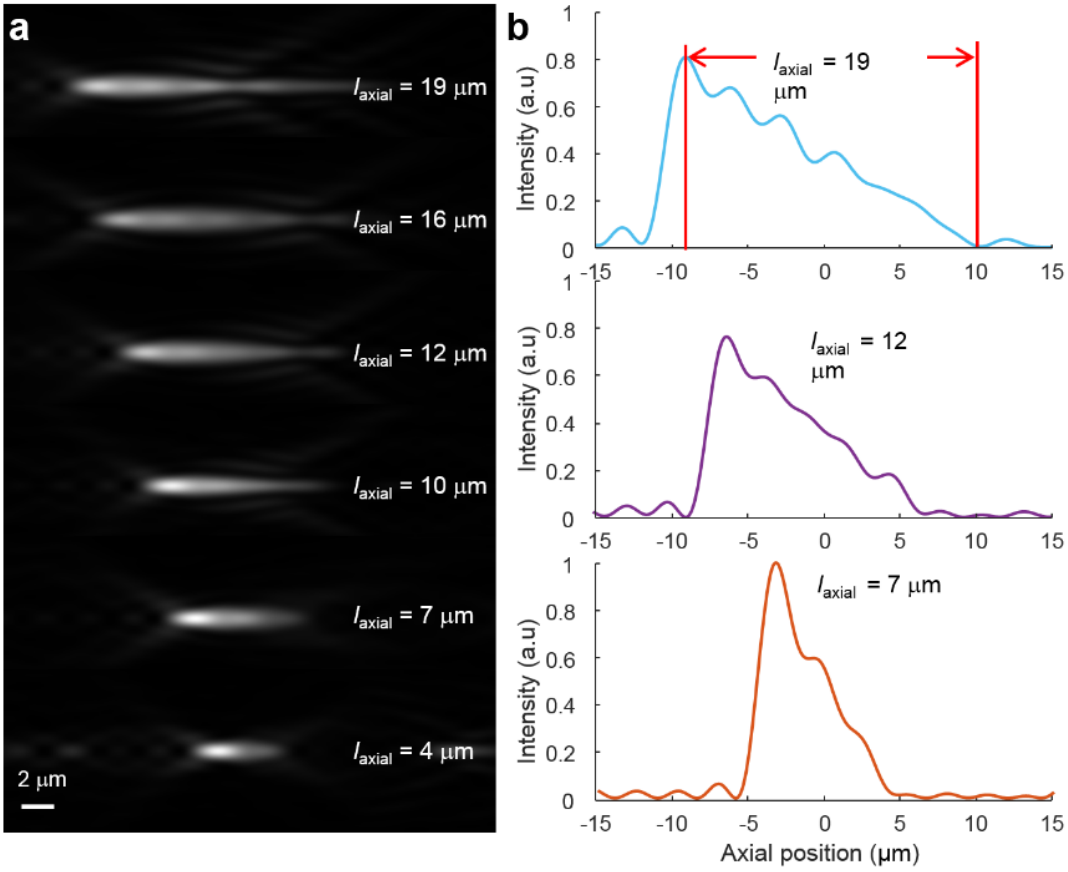


**Fig. S4** Gradient foci with different lengths. (**a**) Theoretical intensity distributions calculated using Richards–Wolf theory and varied from 4 to 20 in focal region. Scale bar, 2 μm. (**b**) Corresponding profiles of 7, 12, and 19 μm gradient foci along optical axis. These profile indicate that 12 μm is favorable for Grad-TPM considering smoothness of slope, maximum intensity, and focal length.

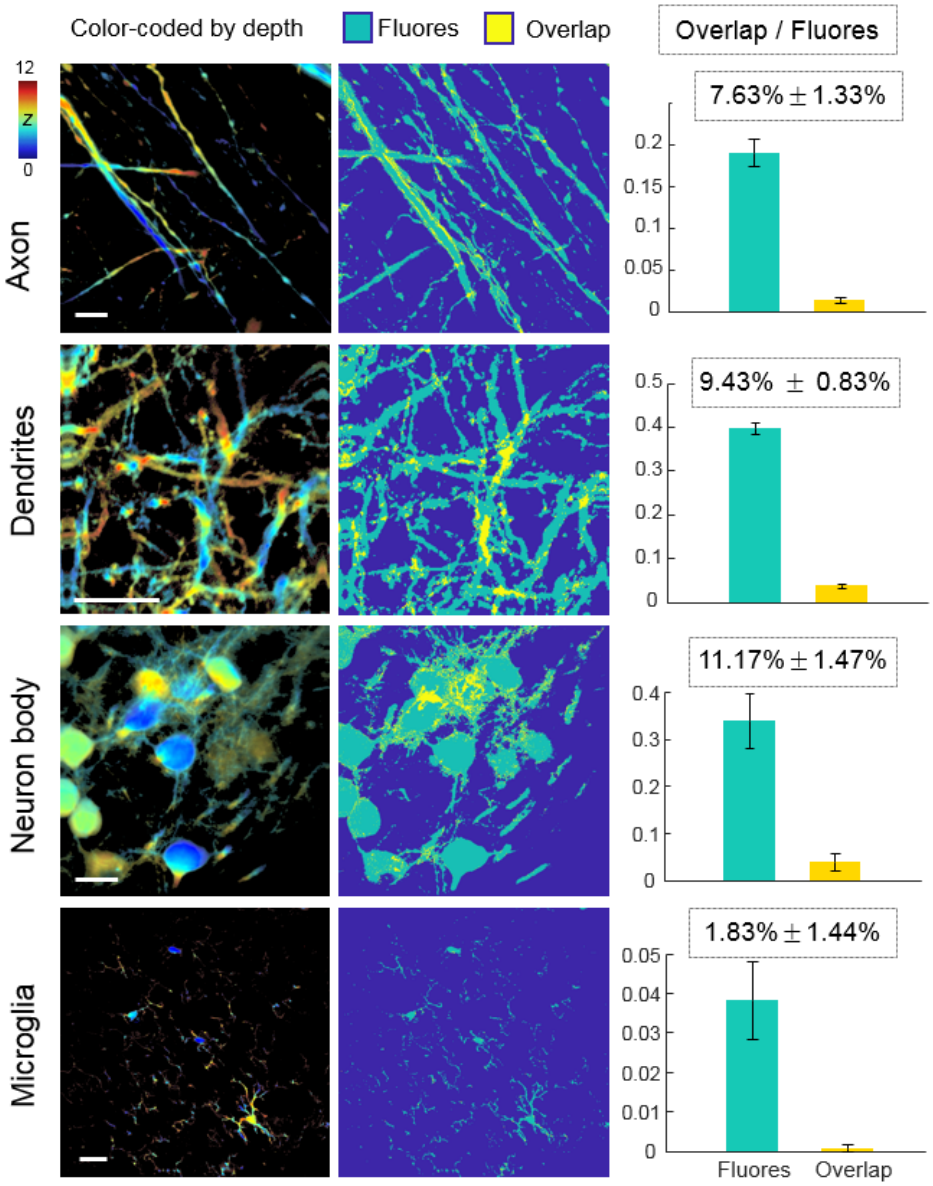


**Fig. S5** Evaluation of the axial overlap of different cellular structures in brain slices. Fluores: fluorescent structures; Overlap, where two or more structures overlaps within the 12-μm axial range. The ratio of the overlap area to the total fluorescent area (measured on Gauss-TPM images) ranges from 1.83% to 11.17%, suggesting that many structures are sparsely distributed in the 12-μm axial range. Therefore, the Grad-TPM method is suitable for imaging brains slices. Unit of $z$: μm.

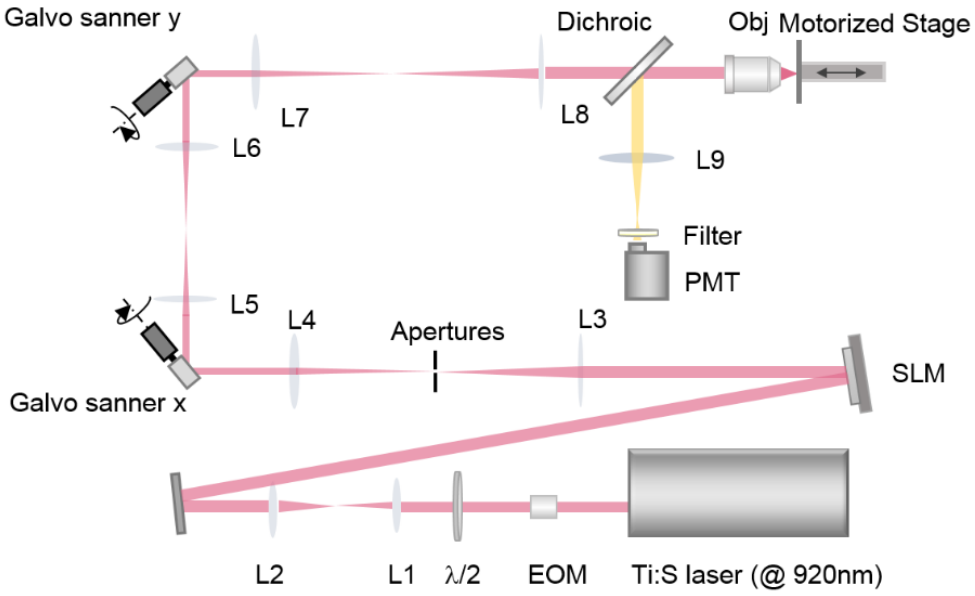


**Fig. S6** Gradient two-photon excitation microscope setup. EOM, electro–optical modulator; λ/2, 1/2 λ wave plate; L, lens; SLM, spatial light modulator; Obj, objective lens; PMT, photomultiplier.

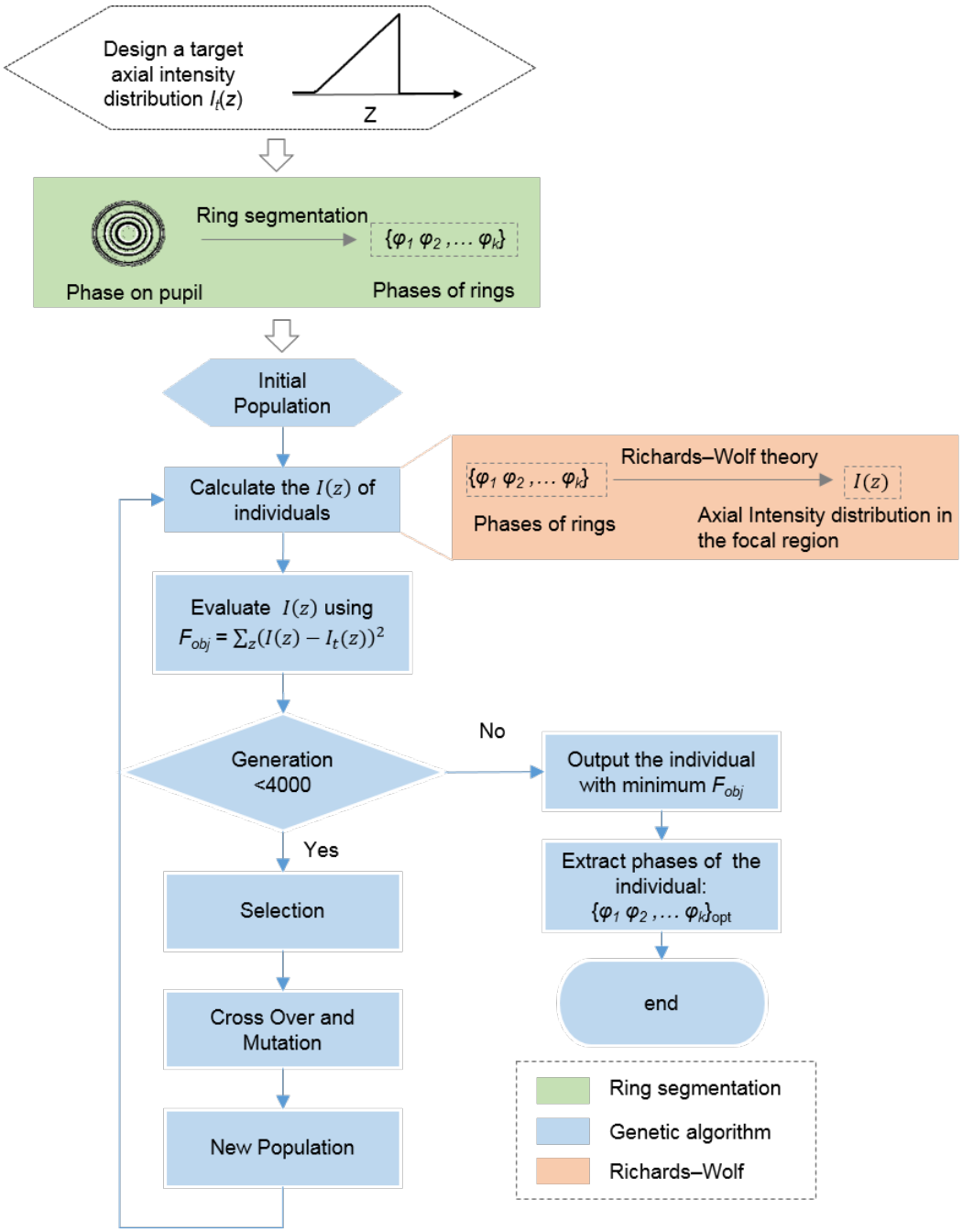


**Fig. S7** Gradient focus generation flowchart. $I_t(z)$: the target axial excitation intensity profile; $I(z)$: the axial excitation intensity profile calculated with the pupil phase $\{\varphi_1 \varphi_2, \ldots \varphi_k\}$, and $\{\varphi_1 \varphi_2, \ldots \varphi_k\}$ denote the phase of each ring on the pupil; $F_{obj}$: the objective function to evaluate the fitness of $I(z)$ and used for individual selection; $\{\varphi_1 \varphi_2, \ldots \varphi_k\}_{opt}$ is the optimal pupil phase generating target gradient focus.

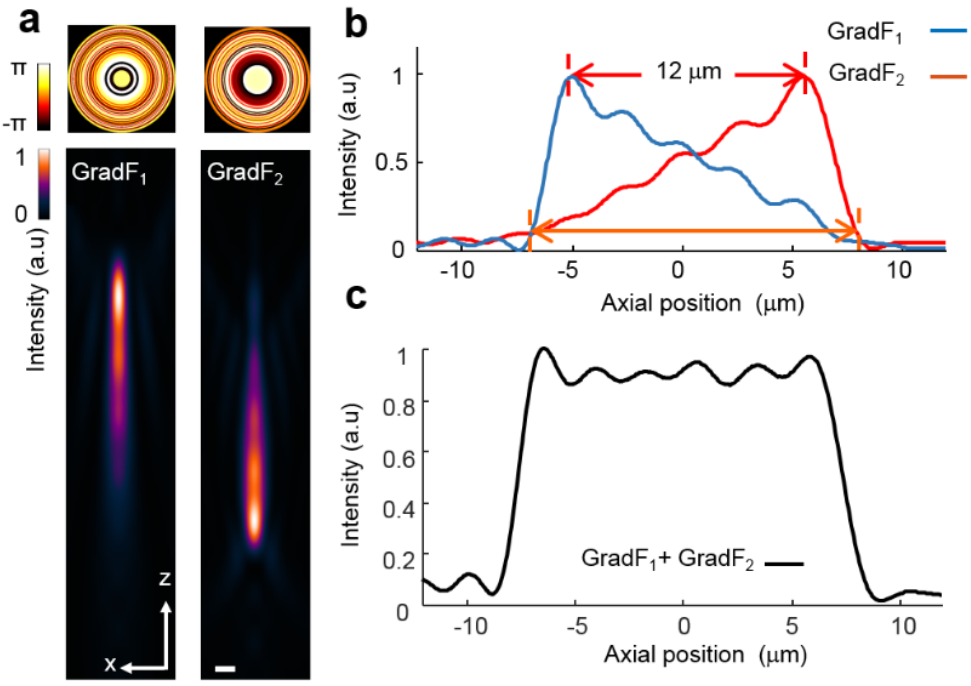


**Fig. S8** Simulated gradient excitation focus pair. (**a**) Axial views of PSFs of the gradient excitation focus pair ($GradF_1$ and $GradF_2$) and corresponding phase patterns that generate the PSFs. Scale bar, 1 μm. (**b**) Intensity profiles of the two gradient excitation foci along the optical axis. (**c**) Sum of the axial intensity profiles of gradient excitation focus pair.

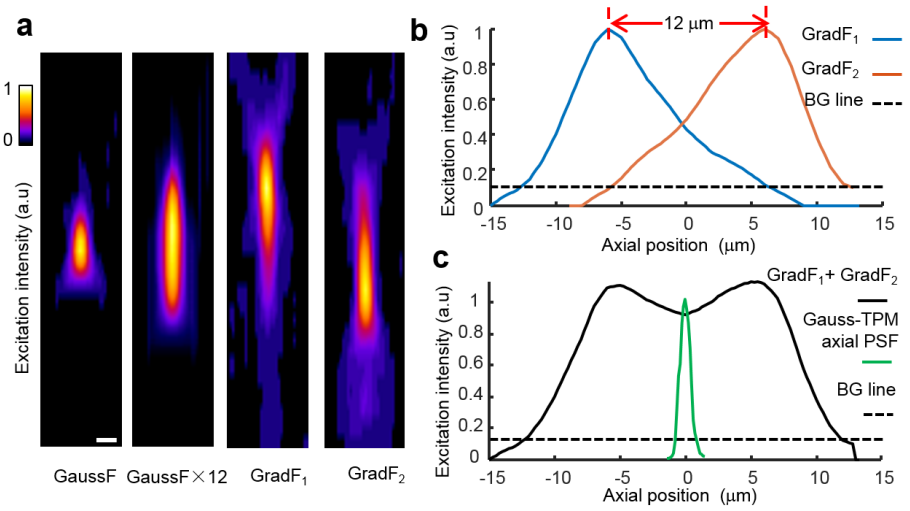


**Fig. S9** Experimental gradient focus pair measured using 1-μm-diameter fluorescent beads. (**a**) Axial-view images of 1 μm fluorescent bead indicating excitation PSFs of Gaussian focus (GaussF), axially cascaded Gaussian foci (GaussF × 12), gradient foci 1 and 2 ($GradF_1$ and $GradF_2$, respectively) from left to right. Scale bar, 1 μm. Note that given the nonlinear effect of two-photon excitation, the emission intensity of the beads was translated to excitation intensity for display. (**b**) Measured excitation intensity profiles of $GradF_1$ and $GradF_2$ along optical axis. (**c**) Measured axial excitation intensity profile of sum of $GradF_1$ and $GradF_2$. The profile of Gaussian focus was also presented for comparison. BG: background.

We measured the PSF of the gradient focus by performing a 3D scanning of a 1-μm-diameter bead within a voxel size of 0.25 μm × 0.25 μm × 1 μm. Because the PSF was undersampled in the axial direction, the resulting PSF was interpolated linearly along the optical axis by a factor of four and then filtered by a 3D Gaussian blur with a radius of one voxel. The square root of the obtained images was used to determine the actual distribution of the excitation light around the focus because the intensity of two-photon excitation fluorescence is proportional to the square of the excitation intensity.

As shown in **b,** the gradient focus exhibits an intensity tail (at the maximum-intensity end) outside the designed axial range. Although we attempted to create an extremely steep tail, some outside fluorophores may still be excited, and their axial locations will be incorrectly estimated. To alleviate this effect, we first adjusted the axial displacement between the pair of foci such that the excitation intensity of one focus is sufficiently small outside the designed axial range. Subsequently, a threshold (BG line in **b**) was empirically selected to exclude the outside fluorophores. Hence, the outside fluorophores excited by the tail at the maximum-intensity end of a focus were located outside of the minimum-intensity end of another focus (under the BG line). These fluorophores will yield an outlier intensity ratio when one of the pairs of intensities becomes negligible. Finally, we carefully determined the intensity ratio range corresponding to the designed axial range and ascribed the fluorophore with an outlier intensity ratio to the nearest available position (top or bottom).

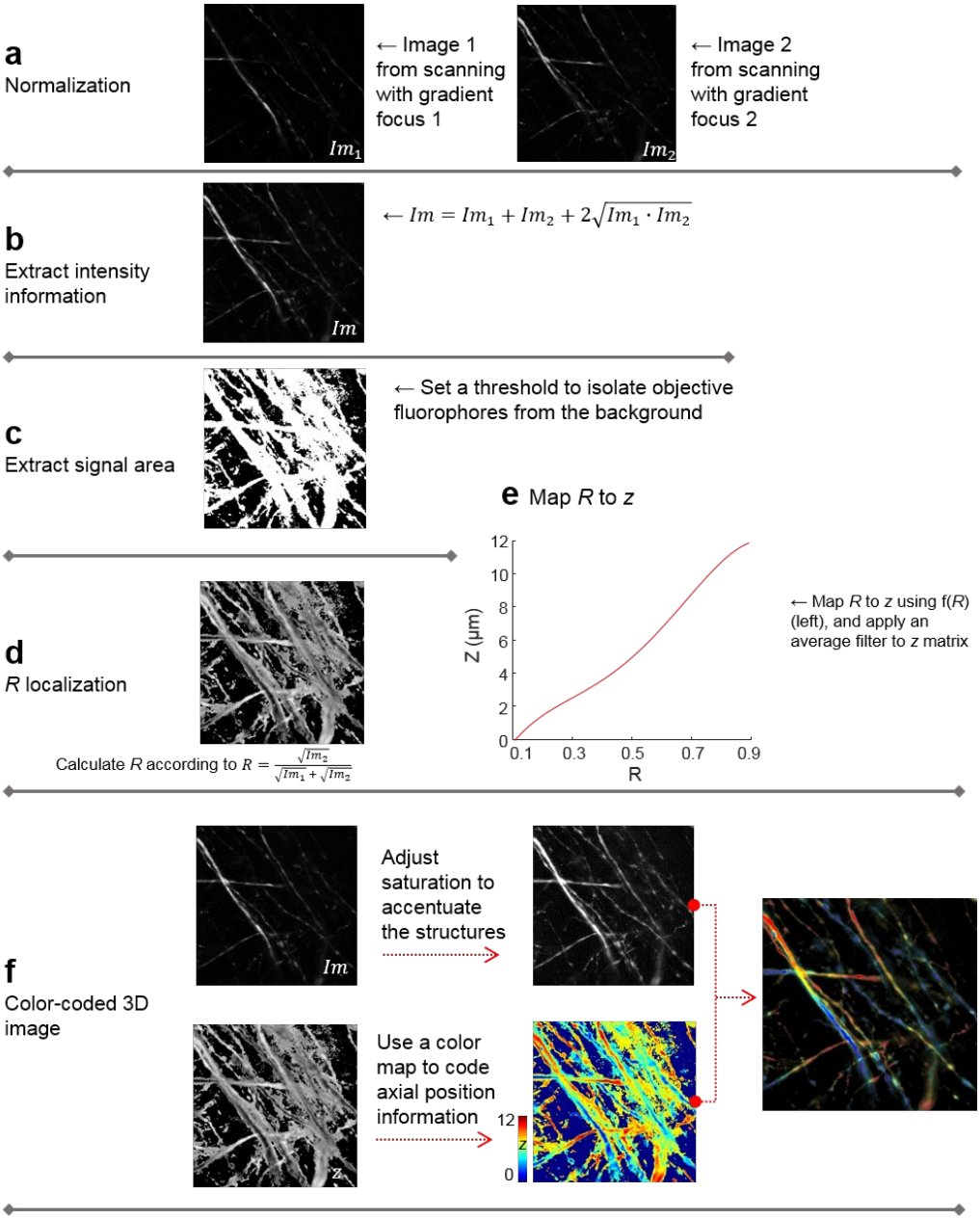


**Fig. S10** Flowchart for axial location information extraction. $Im_1$ and $Im_2$ are paired images that generated by sequentially scanning with the gradient focus 1 and 2; $R$ is the intensity ratio of $Im_1$ to $Im_2$. Function $f(R)$ is a ratio-depth mapping function, which maps $R$ to $z$. Unit of $z$: μm.

# **Table S1.** Data acquisition parameters

| Sample | Figures and Movies | Imaging mode | Single volume acquisition time (s) | Delay between successive acquisitions (s) | Volumetric imaging speed (Hz) | Volume size ($\mu m^3$) | Excitation power (mW) |
|---|---|---|---|---|---|---|---|
| Bead | Fig. 1c-f | Gauss-TPM | 24 | 0 | 0.04 | 50×50×12 | 2 |
| | | Grad-TPM | 4 | 0 | 0.25 | 50×50×12 | 6 |
| Brain slice of $CX_3CR1$-GFP mouse | Fig. 2 | Gauss-TPM | 220 | 0 | 0.0045 | 200×200×22 | 12 |
| | | Grad-TPM | ~37 | 0 | 0.027 | 200×200×22 | ~30 |
| HEK293 cell (photobleaching) | Fig. 3a and Visualization 1 | Gauss-TPM | 13 | 2 | 0.07 | 100×100×13 | ~20 |
| | | Grad-TPM | 2 | 13 | 0.07 | 100×100×12 | 45 |
| RAW264 cell (macrophage) | Fig. 3b and Visualization 3 | Grad-TPM | 8 | 2 | 0.1 | 200×200×12 | 6 |
| HepG2 cell (phototoxicity) | Fig. S3 and Visualization 2 | Gauss-TPM | 52 | 8 | 0.02 | 62.5×62.5×13 | ~20 |
| | | Grad-TPM | 8 | 52 | 0.02 | 62.5×62.5×12 | 45 |

# **Table S2.** Pupil phases of gradient focus pair

| Ring | 1 | 2 | 3 | 4 | 5 | 6 | 7 | 8 | 9 | 10 |
|---|---|---|---|---|---|---|---|---|---|---|
| Outer diameter[a] | $\sqrt{1/40}$ | $\sqrt{2/40}$ | $\sqrt{3/40}$ | $\sqrt{4/40}$ | $\sqrt{5/40}$ | $\sqrt{6/40}$ | $\sqrt{7/40}$ | $\sqrt{8/40}$ | $\sqrt{9/40}$ | $\sqrt{10/40}$ |
| Phase of $GradF_1$[b] | 2.90 | 1.07 | -1.88 | 2.25 | 1.15 | -1.20 | -2.53 | 1.17 | -2.67 | -1.32 |
| Phase of $GradF_2$[b] | 3.07 | 1.00 | -2.55 | -1.49 | 1.84 | -1.07 | -2.11 | -0.04 | 0.38 | -1.22 |

| Ring | 11 | 12 | 13 | 14 | 15 | 16 | 17 | 18 | 19 | 20 |
|---|---|---|---|---|---|---|---|---|---|---|
| Outer diameter | $\sqrt{11/40}$ | $\sqrt{12/40}$ | $\sqrt{13/40}$ | $\sqrt{14/40}$ | $\sqrt{15/40}$ | $\sqrt{16/40}$ | $\sqrt{17/40}$ | $\sqrt{18/40}$ | $\sqrt{19/40}$ | $\sqrt{20/40}$ |
| Phase of $GradF_1$ | 2.48 | 2.85 | -2.23 | -2.55 | 2.23 | -2.67 | -0.95 | 2.99 | -1.81 | -0.87 |
| Phase of $GradF_2$ | 1.10 | -0.23 | 1.10 | 2.48 | 0.97 | 2.01 | 2.45 | 2.38 | 2.85 | 2.94 |

| Ring | 21 | 22 | 23 | 24 | 25 | 26 | 27 | 28 | 29 | 30 |
|---|---|---|---|---|---|---|---|---|---|---|
| Outer diameter | $\sqrt{21/40}$ | $\sqrt{22/40}$ | $\sqrt{23/40}$ | $\sqrt{24/40}$ | $\sqrt{25/40}$ | $\sqrt{26/40}$ | $\sqrt{27/40}$ | $\sqrt{28/40}$ | $\sqrt{29/40}$ | $\sqrt{30/40}$ |
| Phase of $GradF_1$ | -1.98 | -1.54 | -1.24 | -2.70 | -1.86 | -3.07 | 2.90 | 2.80 | 2.48 | 2.08 |
| Phase of $GradF_2$ | -3.14 | -2.65 | -1.49 | -2.67 | -1.61 | -1.47 | -2.65 | -0.87 | -2.67 | -2.01 |

| Ring | 31 | 32 | 33 | 34 | 35 | 36 | 37 | 38 | 39 | 40 |
|---|---|---|---|---|---|---|---|---|---|---|
| Outer diameter | $\sqrt{31/40}$ | $\sqrt{32/40}$ | $\sqrt{33/40}$ | $\sqrt{34/40}$ | $\sqrt{35/40}$ | $\sqrt{36/40}$ | $\sqrt{37/40}$ | $\sqrt{38/40}$ | $\sqrt{39/40}$ | 1 |
| Phase of $GradF_1$ | 2.01 | 1.86 | 1.00 | 1.32 | -0.75 | 0.90 | -0.95 | -1.52 | 0.97 | -2.53 |
| Phase of $GradF_2$ | -3.09 | -2.94 | -2.38 | 2.85 | -2.21 | -2.55 | 0.87 | -2.77 | 0.95 | 2.16 |

a: Normalized value.

b: $GradF_1$, gradient focus 1; $GradF_2$, gradient focus 2.

# **Note S1.** Grad-TPM imaging of axially overlapping structures

It should be noted that we used the same algorithm (Eq. 2 and Section 4.3) for both overlapping and non-overlapping areas. This algorithm provides a weighted average axial location for axially-overlapped objects. The weight is the fluorescence intensity of each object within the 12-μm range. As a result, the *z*-coded *x*-*y* projection image obtained using Grad-TPM is almost the same as that obtained using Gauss-TPM (Fig. 2a). But in the reconstructed 3D Grad-TPM image, the overlapped objects will be axially misplaced. We demonstrated this point by simulating two dendrites crossing each other at different depths. Since axial localization of Grad-TPM involves two variables: fluorescence intensity and axial position, we performed the simulation in two cases: (1) two fibers with the same intensity but different axial locations (Fig. N1a); (2) two fibers with different fluorescence intensities but constant axial locations (Fig. N1b). The 3D reconstructions of the overlapping fibers were shown in Figs. N1c-f. Actually, we can estimate the axial location of each overlapped object using the axial locations of nearby non-overlapping areas, according to the continuity of biological structures (Fig. N1g). Since it doesn't make sense for *z*-coded *x*-*y* projection images, we didn't use the strategy in this study. But it will play an important role in future 3D reconstruction of Grad-TPM images.

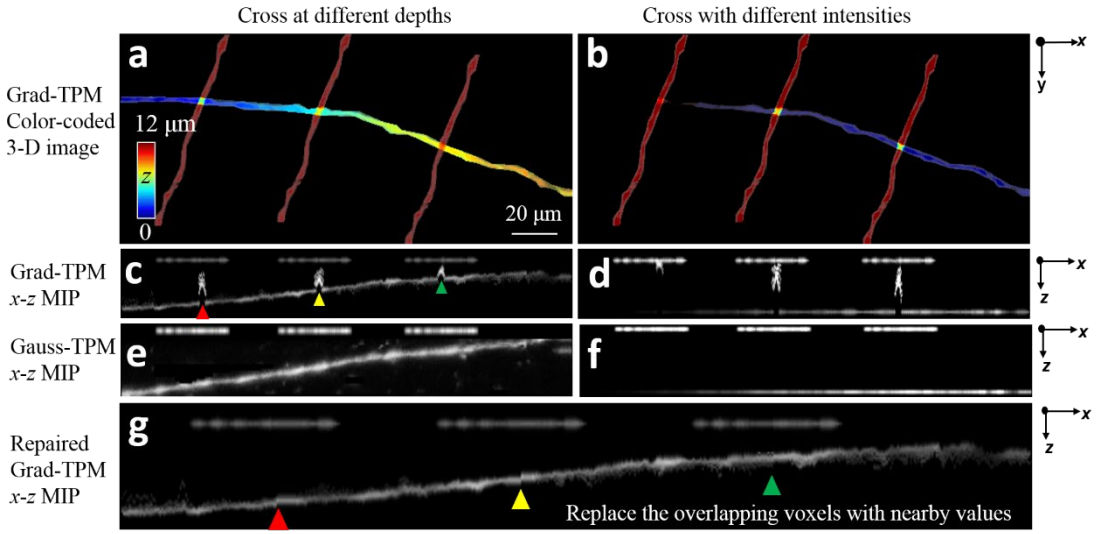


**Fig. N1** Grad-TPM volumetric reconstructions of axially overlapping fibers. (**a**) Color-coded 3D Grad-TPM image of fibers overlapping at different depths. (**b**) Color-coded 3D Grad-TPM image of overlapping fibers with different intensities. (**c,d**). *x*-*z* maximum intensity projection(MIP) of the reconstructed volume presented in **a** and **b**, respectively. (**e,f**). Ground truths of **c** and **d** that obtained with Gauss-TPM. (**g**) Repaired *x*-*z* MIP corresponding to **c**. The axial locations of misplaced voxels were replaced with those of their nearby non-overlapping areas.

# **Note S2.** Evaluation of axial localization error caused by fluorescence intensity fluctuation

Noise, photobleaching, as well as fluorescence changes (such as calcium activity) all directly cause fluorescence intensity fluctuation and consequently lead to axial localization error in Grad-TPM. Here, we calculated the tolerable fluorescence intensity fluctuation using uncertainty propagation(*http://ipl.physics.harvard.edu/wp-uploads/2013/03/PS3_Error_Propagation_sp13.pdf*). According to Eq. 2, the axial location of a fluorophore $z$ can be simply expressed as

$$z \approx lR = l\frac{\sqrt{Im_2}}{\sqrt{Im_1}+\sqrt{Im_2}} = l\frac{1}{\sqrt{Im_1/Im_2}+1}, \tag{N1}$$

where $l$ is the axial length of the gradient foci, i.e. 12 μm; $R$ is the ratio of excitation intensity of $Im_2$ to the total; $Im_1$ and $Im_2$ are fluorescence images corresponding to gradient focus 1 and 2, respectively. According to rules of uncertainty propagation, the uncertainty of $z$, namely $\delta z$, can be expressed as

$$\delta z = \frac{l}{2}\sqrt{\left(\frac{\delta Im_1}{Im_1}\right)^2+\left(\frac{\delta Im_2}{Im_2}\right)^2}\,\frac{\sqrt{Im_1 Im_2}}{\left(\sqrt{Im_1}+\sqrt{Im_2}\right)^2}, \tag{N2}$$

where $\delta Im_1$ and $\delta Im_2$ are uncertainties of $Im_1$ and $Im_2$, respectively. Theoretically, $\delta Im$ ($\delta Im_1$ or $\delta Im_1$) between frames (1 Hz frame rate) is acceptable, as long as $\delta z$ caused by them is within the axial localization precision of the Grad-TPM (0.63 μm), namely,

$$\frac{l}{2}\sqrt{\left(\frac{\delta Im_1}{Im_1}\right)^2+\left(\frac{\delta Im_2}{Im_2}\right)^2}\,\frac{\sqrt{Im_1 Im_2}}{\left(\sqrt{Im_1}+\sqrt{Im_2}\right)^2} \le 0.63 \tag{N3}$$

Since the range of $\frac{\sqrt{Im_1 Im_2}}{\left(\sqrt{Im_1}+\sqrt{Im_2}\right)^2}$ is [0, 0.25] (0 corresponds to the depth of 0 μm or 12 μm, 0.25 corresponds to the depth of 6 μm), we can deduce that

$$\left(\frac{\delta Im_1}{Im_1}\right)^2+\left(\frac{\delta Im_2}{Im_2}\right)^2 \le 0.1764 \tag{N4}$$

The inequality definitely holds when both $(\delta Im_1/Im_1)^2 \le 0.0882$ and $(\delta Im_2/Im_2)^2 \le 0.0882$. Thus, we can see that the upper limit of acceptable $\delta Im/Im$ is 29.7%/s. This conclusion was further confirmed through our simulation experiment. We assumed that the intensity of the Grad-TPM image pair randomly fluctuates within the range of ±29.7% and calculated corresponding localization errors. The results show that the errors are within ±0.63 μm (Fig. N2).

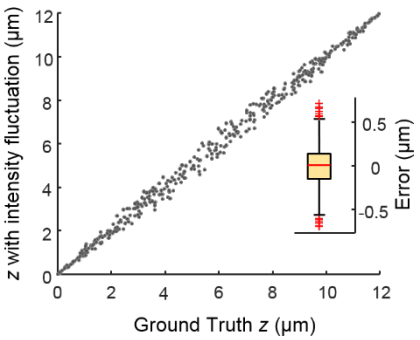


**Fig. N2** Localization error caused by random fluorescence intensity fluctuation within ±29.7% (n=400).